Catalysis Letters (2019) 149:2575–2585
https://doi.org/10.1007/s10562-019-02874-9

2-Methylimidazole Modified Co-BTC MOF as an Efficient Catalyst for Chemical Fixation of Carbon Dioxide

Yuanfeng Wu[1] · Xianghai Song[1] · Siquan Xu[1] · Jiahui Zhang[1] · Yanli Zhu[1] · Lijing Gao[1] · Guomin Xiao[1]

Received: 30 April 2019 / Accepted: 17 June 2019 / Published online: 22 June 2019

Abstract

$[(CH_3)_2NH_2][Co_3(BTC)(HCOO)_4(H_2O)]\cdot H_2O$ (Co-BTC) was synthesized under solvothermal conditions, further used as the precursor for the synthesis of 2-methylimidazole modified Co-BTC (2MeIm@Co-BTC-*x*). The characteristics of 2MeIm@Co-BTC-*x* were systematically characterized by various technologies including XRD, FESEM, FT-IR, XPS, N_2-adsorption, TG-DTG and CO_2/NH_3-TPD. It was found that except for the crystal faces (0 1 1) and (− 1 0 2) corresponding to ZIF-67 and Co-BTC, a new crystal phase appeared at 12.22° for the modified Co-BTC, which may be attributed to the coordination between 2MeIm and unsaturated Co ions of Co-BTC. Interestingly, a new structure of hexagonal prisms together with hierarchical porous were also formed for the modified Co-BTC. Besides, when this composite was explored as a heterogeneous catalyst for catalytic conversion of carbon dioxide with epichlorohydrin (ECH) as probe, an obvious enhancement in catalytic activity was obtained compared with the fresh Co-BTC, suggesting that 2MeIm ligands within the modified Co-BTC played a great role on the coupling process. Furthermore, 97.21% of ECH conversion and 98.79% of chloropropene carbonate selectivity were gained over 2MeIm@Co-BTC-1.0 under optimal conditions (3.0 MPa, 90 °C, 5 h, 0.75 wt% catalyst of ECH). Additionally, only a slight decrease in catalytic activity was found after the optimal sample was reused three times. Finally, a mechanism for interpreting the coupling process of carbon dioxide cycloaddition with epoxide was proposed.

Graphic Abstract

One-pot catalytic conversion of CO2 into cyclic carbonate over 2-methylimidazole modified Co-BTC

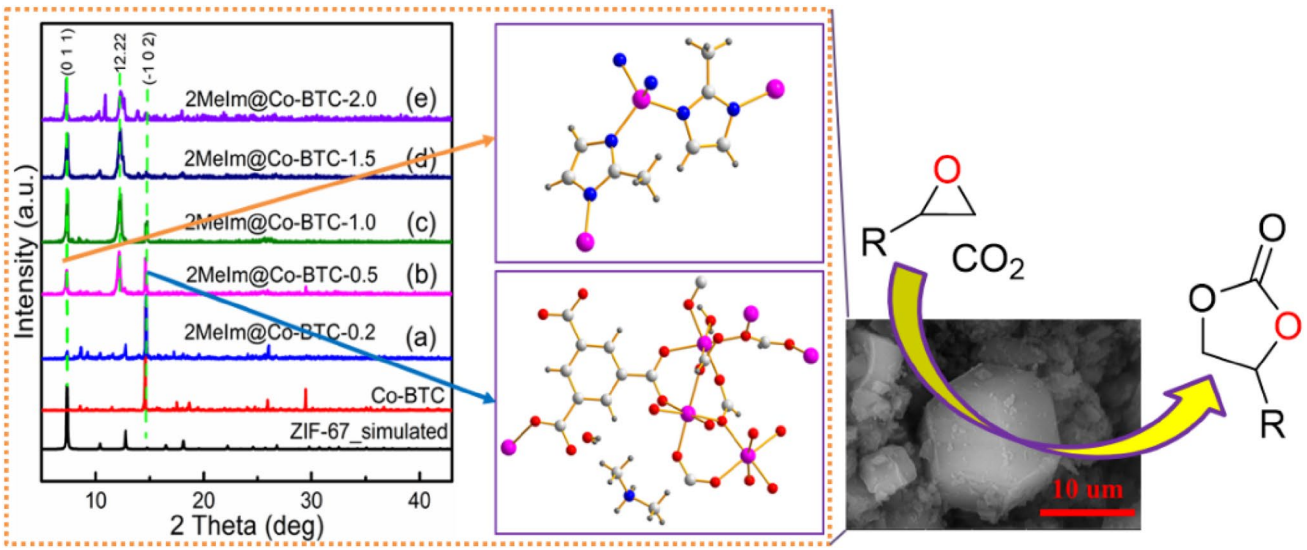

Electronic supplementary material The online version of this article (https://doi.org/10.1007/s10562-019-02874-9) contains supplementary material, which is available to authorized users.

Extended author information available on the last page of the article

Keywords ZIF-67 · Co-BTC · CO_2 · Epoxide · Cycloaddition

1 Introduction

Recently, the increasing emission of carbon dioxide from fuel combustion has brought in a series of serious effects on climate, of which glaciers sharply decreases followed with global warming [1–3]. Such changes have spurred numerous researchers in the past to explore the conversion technologies for carbon dioxide utilization. As a result, some methods have been developed for fine chemicals synthesis with carbon dioxide as the staring material [4–6]. For instance, efficient conversion of carbon dioxide into methyl *N*-phenylcarbamate has been performed in the presence of *n*-butyllithium [7], and synthesis of diphenyl carbonate with CO_2 as the substrate was also explored under the methanol atmosphere [8]. Besides, carbon dioxide was also fixed chemically with the Aziridines as the coupling reagent [9]. In addition, one-pot synthesis of cyclic carbamates from aminoalcohols and carbon dioxide was also investigated with acetonitrile as solvent [10]. Besides, when ceria-calcium bimetal oxides were employed, carbon dioxide can be efficiently converted into dimethyl carbonate [11]. Nevertheless, efficient production of cyclic carbonates (Scheme 1) via cycloaddition of carbon dioxide to epoxides become increasingly interesting due to the wide application of the products in industries [12–15].

Up to now, various compounds such as ionic liquids [16–18], alkali metal halides [19, 20], boron phosphate [21], functional polymer [22], and quaternary ammonium or phosponium salts [23, 24], have been widely employed as homogenous catalysts for the acceleration of carbon dioxide insertion into epoxide. However, the process for separating the used catalyst was difficult to preform and the subsequent treatments were also relatively complicated. On the other hand, some catalysts such as wool powder-KI [25], metal salen complexes [26, 27] and metal oxides [28] were also widely adopted for the synthesis of cyclic carbonates. However, most cases were performed in the presence of co-catalyst or/and organic solvents under the high reaction temperature and pressure. As a result, some efforts have been devoted to explore the relative mild reaction conditions for efficient conversion of CO_2 into cyclic carbonates.

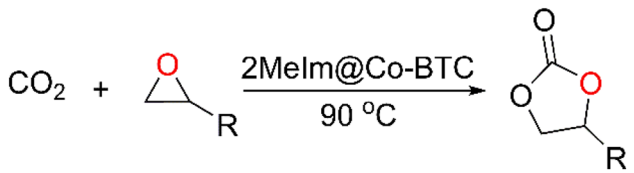

Scheme 1 Catalytic conversion of CO_2 into cyclic carbonates over 2-methylimidazole modified Co-BTC

Some metal–organic framework materials have been employed for carbon dioxide cycloaddition due to the presence of Lewis or/and Brønsted acid sites inside the crystal structure. For example, zirconium-based isoreticular MOFs and the co-catalyst (TBAB) have been investigated to possess the synergistical catalysis for cyclic carbonates synthesis [29]. When the MOF-5 and n-Bu_4NBr were simultaneously added in the catalytic system, the conversion of propylene oxide was obviously enhanced compared with that of signal MOF-5 [30]. Besides, efficient production of chloropropene carbonate from carbon dioxide was widely explored with various materials such as ZIF-67 [31], ZIF-8 [32] as well as amine-modified MIL-101 [33] and MIL-125 [34]. Additionally, when the Zn-doped ZIF-67 was employed in the catalytic system, an obvious enhancement in the conversion of epichlorohydrin was observed compared with the free ZIF-67 [35]. It can be drawn that some MOFs can become more efficient in conversion of carbon dioxide after modified with active groups.

The MOFs of $[(CH_3)_2NH_2][Co_3(BTC)(HCOO)_4(H_2O)]\cdot H_2O$ (Co-BTC) was previously explored for CO_2 conversion, but a low conversion of ECH was observed at the harsh reaction conditions(120 °C, 9 h) [36]. However, 2MeIm has been explored with the highly-efficient activity for chemical fixation of CO_2, but difficult to be reused. Fortunately, Co ions can coordinate with 2MeIm ligands to form ZIF-67 which can be easily regained via filtration.

Therefore, the present work aimed to modify Co-BTC with active groups, impacting the Co-BTC with higher catalytic activity for CO_2 conversion. As a result, a new material was designed and prepared via grafting 2MeIm onto the surface of Co-BTC that 2MeIm was linked to the unsaturated Co ions of Co-BTC. In this work, 2MeIm modified Co-BTC was synthesized under the solvothermal conditions, and further exploited as a catalyst for efficiently converting carbon dioxide into cyclic carbonates. Besides, various reaction parameters as well as probe molecules were investigated for achieving the optimal reaction conditions and coupling scope. Experimental section can be found in the supporting information.

2 Results and Discussion

2.1 Characterization of the Modified Co-BTC

XRD patterns of 2MeIm modified Co-BTC were presented in Fig. 1. The peaks located at 12.1° (0 1 1) and 14.7° (− 1 0 2) correspond to the characteristic patterns of ZIF-67 [37] and Co-BTC [36], respectively. Besides, a new crystal

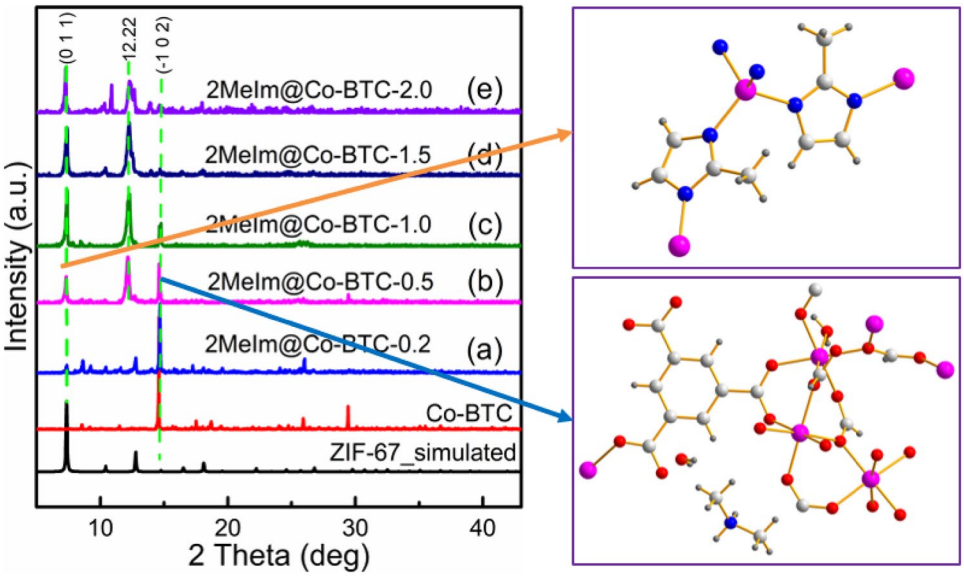

Fig. 1 PXRD patterns of the modified BTC samples, **a** 2MeIm@Co-BTC-0.2, **b** 2MeIm@Co-BTC-0.5, **c** 2MeIm@Co-BTC-1.0, **d** 2MeIm@Co-BTC-1.5, **e** 2MeIm@Co-BTC-2.0

phase was also found at 12.22° for the modified Co-BTC. This newly-formed phase may be due to the 2MeIm ligands being linked to the cobalt ions, thereby forming a special structure onto Co-BTC surface. The intensity of (− 1 0 2) crystal phase associated with Co-BTC gradually decreases while that of (0 1 1) assigned to ZIF-67 obviously increases with the increase in mass ratio (*x*) of 2MeIm/Co-BTC. Such changes were likely due to the newly-formed phase associated with enhanced ZIF-67, which made the surface of Co-BTC increasingly covered during the solvothermal process.

FESEM images of 2-methylimidazole modified Co-BTC were shown in Fig. 2. It can be seen that irregular microstructure was observed for the Co-BTC (Fig. 2a–c). When the crystal material was modified by 2MeIm, a new structure of hexagonal prisms appeared onto the Co-BTC surface (Fig. 2d–f). This new appearance might be associated with the coordination between 2MeIm ligands and unsaturated Co ions.

N_2-adsorption–desorption isotherms of 2MeIm modified Co-BTC were exhibited in Fig. S1a. The modified Co-BTC samples depicted the diagrams combining both of Types I and IV characteristics, illustrating the presence of micro- and meso-poros inside the solid [38]. Besides, the total surface area (BET) was measured to be more highly compared with micropore surface area as determined by t-plot method (Table 1). Thus, such likely behavior could be related to the presence of meso-porous in the modified samples, which was further evidenced by the results of BJH pore size distribution (Fig. S1b). In addition, the surface area (BET) of the modified Co-BTC firstly increases from 118 $m^2\ g^{-1}$ ($x = 0.2$) to 428 $m^2\ g^{-1}$ ($x = 1.0$) and then decreases to 245 $m^2\ g^{-1}$ ($x = 1.5$), and finally exhibited an increasing trend (358 $m^2\ g^{-1}$, $x = 2.0$). Moreover, a similar change was also observed in total pore volume. Furthermore, the average pores size continuously increases and maximizes to 11.8 nm, and then exhibited a downward trend. It is likely that 2MeIm ligand linked with Co ions only existed on the surface of Co-BTC at a low mass ratio. At a high mass ratio ($x > 1.0$), such coordination may have occurred within the internal structure, and as a result, the phase of (0 1 1) associated with ZIF-67 (Fig. 1) was enhanced with the increasing mass ratio. For 2MeIm@Co-BTC-1.0, the high pores size was formed within the crystal structure, implying that the reactants and products could diffuse more easily through the pore structure.

FT-IR spectrums of 2MeIm@Co-BTC were exhibited in Fig. 3. The broad adsorption band assigned to -OH groups was detected in the corresponding range of 3600–3000 cm^{-1} [39], suggesting that some water molecules existed in the crystal structure. However, the band of H_2N^+ groups was barely observed in the region of 2890–2780 cm^{-1}, which may be due to the loss of $[(CH_3)_2NH_2]^+$ cations in the crystal structure. The absorption band of the carboxylate groups appeared in the region of 1645–1550 cm^{-1} (asymmetric vibration) and 1440–1390 cm^{-1} (symmetric vibration) instead of 1800–1680 cm^{-1} [40, 41], indicating that the –COOH groups could have completely coordinated with cobalt ions [42]. The bands relating to C–C groups (1100 cm^{-1}) and C–H groups (866–715 cm^{-1}) of benzene ring (fresh Co-BTC) [43] were respectively detected at 1128 cm^{-1} and 796–715 cm^{-1} for the modified Co-BTC. It is possible that such shift was due to the reason that 2MeIm ligands have coordinated with the unsaturated cobalt ions, thereby forming a special bond between 2MeIm and BTC linked via the Co bridge.

The chemical state of 2MeIm modified Co-BTC were determined by XPS. As exhibited in Fig. 4a, the signals representing the four kinds of elements were detected at

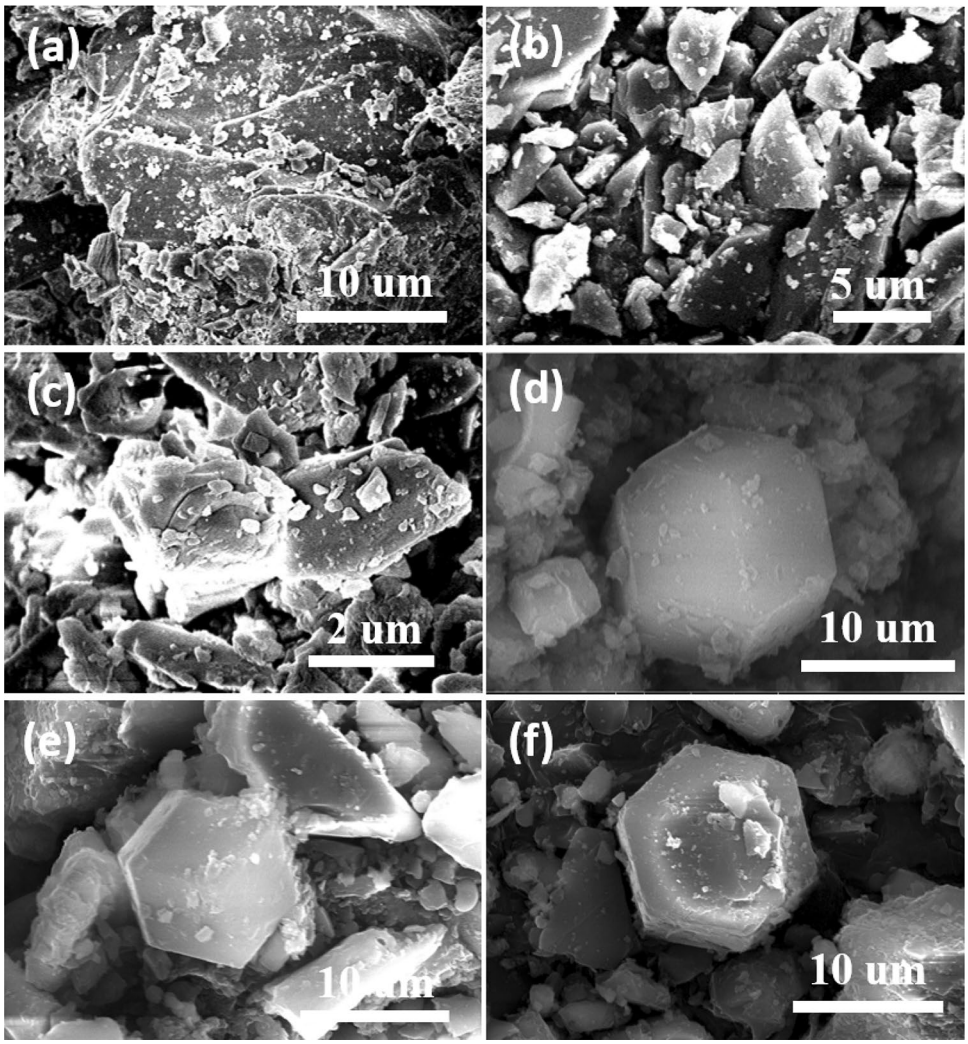

Fig. 2 FESEM images of **a–c** Co-BTC and **d–f** 2MeIm@Co-BTC-1.0 samples

Table 1 Textural properties of 2MeIm modified Co-BTC

Samples	S^{a}_{BET} ($m^2\ g^{-1}$)	S^{c}_{micro} ($m^2\ g^{-1}$)	S^{c}_{meso} ($m^2\ g^{-1}$)	V^{b}_{total} ($m^3\ g^{-1}$)	V^{c}_{micro} ($m^3\ g^{-1}$)	D_{avera} (nm)
2MeIm@Co-BTC-0.2	118	37	81	0.130	0.020	6.63
2MeIm@Co-BTC-0.5	175	111	64	0.195	0.059	9.36
2MeIm@Co-BTC-1.0	428	371	56	0.347	0.190	11.78
2MeIm@Co-BTC-1.5	245	126	119	0.285	0.066	8.25
2MeIm@Co-BTC-2.0	358	250	107	0.458	0.128	4.89

[a]BET method

[b]Volume adsorbed at $p/p_0 = 0.98$

[c]*t*-plot method

284.8 eV (C 1s), 400.0 eV (N 1s), 532.0 eV (O 1s), and 781.0 eV (Co 2p). However, the intensities of C1s and N1s signal were obviously enhanced compared with that of fresh Co-BTC, while that of O1s signal decreased. Such changes further confirmed that 2MeIm ligands have been linked to unsaturated cobalt ions of Co-BTC. This is also in line with the results of XRD (Fig. 1) and FT-IR (Fig. 3). The C 1s spectrum of the Co-BTC sample was substituted with several symmetrical peaks (Fig. 4b) which correspond to the C–C (284.8 eV), C–N (286.1 eV), C–O (286.8 eV), C=O (288.4 eV), and O–C=O (289.2 eV) groups [44]. However, the binding peak associated with the O–C=O groups was not detected for 2MeIm@Co-BTC-1.0. It is likely that the newly-formed structure (Fig. 2) has completely covered the

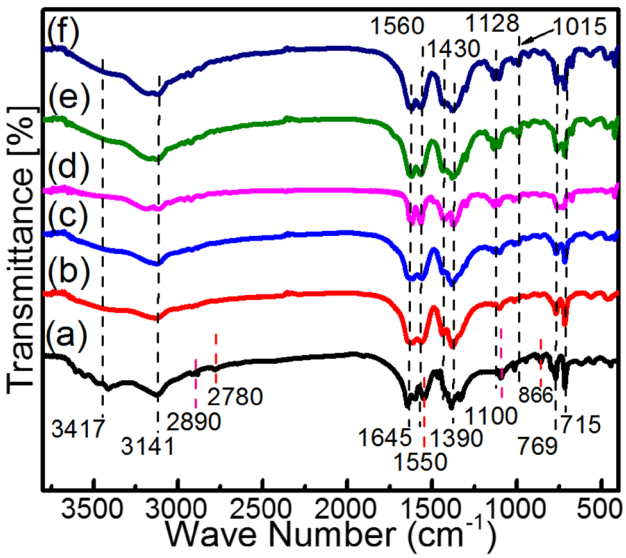

Fig. 3 FT-IR spectra of the 2MeIm@Co-BTC and Co-BTC samples. **a** Co-BTC, **b** MeIm@Co-BTC-0.2, **c** 2MeIm@Co-BTC-0.5, **d** 2MeIm@Co-BTC-1.0, **e** 2MeIm@Co-BTC-1.5, **f** 2MeIm@Co-BTC-2.0

surface of Co-BTC during the preparation process. Two symmetrical peaks were used for the deconvolution of N 1s spectra as shown in Fig. 4c. For Co-BTC, the B.E. centered at 399.6 eV and 401.9 eV were assigned to C–N–C and N–H, respectively [45]. After Co-BTC was modified by 2MeIm, the B.E. of N 1s spectrum shifted downwards, which implied that the newly-formed chemical bond between 2MeIm and unsaturated Co ions exhibited lower binding energy. The symmetrical components and associated satellite line were employed for fitting the Co 2p spectra (Fig. 4d). The coordination modes between Co and O ions for both samples were in a good agreement with each other, suggesting that three coordination modes of Co^{2+} ions (Co1, Co2, Co3) coexisted within the solid [36].

The thermal behaviors of 2MeIm modified Co-BTC were performed under nitrogen atmosphere (Fig. 5). It can be seen that the TG curve consists of four stages based on DTG curve classification. The first-two stages (60–250 °C) were associated with the loss of the adsorbed and the structural water (found at 4.77 wt%, 2.14 wt%), which was slightly lower than that of the Co-BTC, suggesting that some water molecules were released from the crystal structure during the modifying process. The third stage from 250 to 350 °C is ascribed to the release of dimethylamine cation [$(CH_3)_2NH_2^+$) [46], while, the last stage from 350 to 800 °C

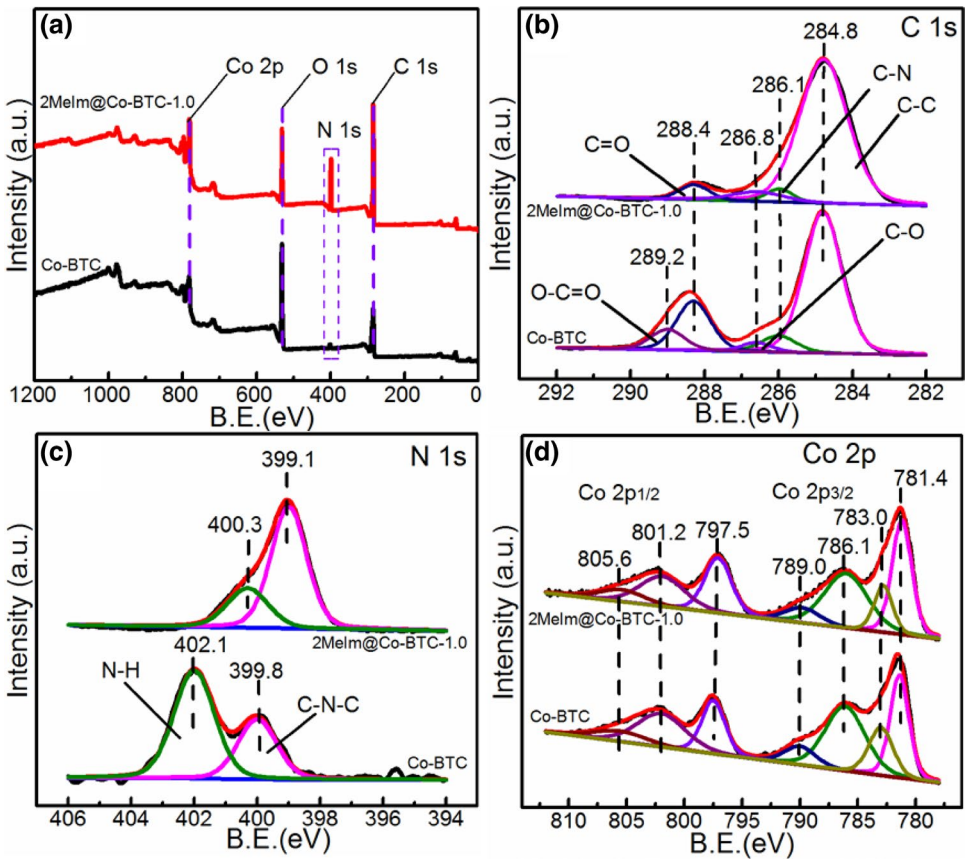

Fig. 4 XPS spectra of the Co-BTC and 2MeIm@Co-BTC-1.0 samples. **a** Full spectra, **b** C1s, **c** N1s, **d** Co 2p

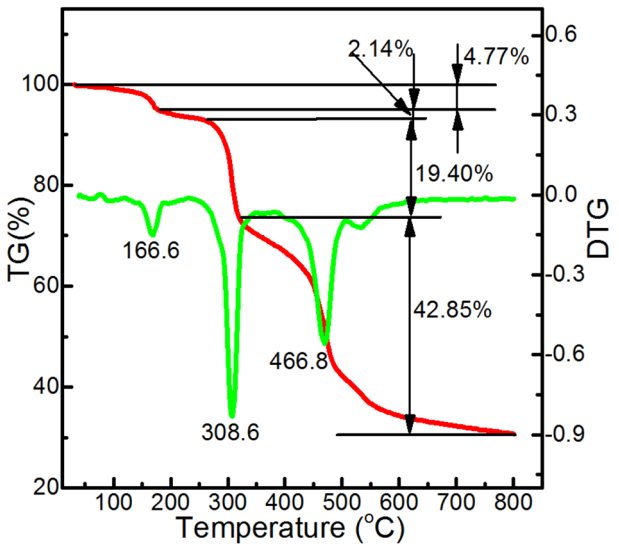

Fig. 5 TG-DTG curves of the 2MeIm@Co-BTC-1.0 sample

was the primary loss of 2MeIm and BTC ligands, forming the corresponding oxide of Co_3O_4.

The TPD profiles of 2MeIm modified Co-BTC were determined under helium atmosphere, with the results displayed in Fig. 6a. The area of NH_3-TPD profile (modified Co-BTC) obviously decreased compared with the fresh Co-BTC sample, suggesting that the cobalt ions, which served as Lewis acid sites, have been released from the crystal structure. Besides, when the desorption temperature increases from 30 to 270 °C, CO_2-TPD curve still maintained a constant, implying that carbon dioxide exhibited difficult dissociation from the nitrogen-containing groups. To validate the existence of strong interaction between carbon dioxide and the modified Co-BTC, CO_2-adsorption was performed (Fig. 6b). For each of the sample, maximum adsorption was obviously enhanced compared with Co-BTC (8.03 ml/g), and gradually increased from 17.50 ml/g ($x = 0.2$) to 23.84 ml/g ($x = 1.0$), followed by decrease to 19.28 ml/g ($x = 1.5$), suggesting that the special structure was formed within the modified Co-BTC ($x = 1.0$). Therefore, 2MeIm modified Co-BTC with Lewis basic-acid sites was confirmed according to the above analysis.

2.2 Carbon Dioxide Coupling with Epichlorohydrin

The ECH conversion as well as the CPC selectivity were employed as the evaluation criterion for exploring the optimal reaction conditions.

The catalytic activity of 2MeIm@Co-BTC was explored for CO_2 conversion with ECH as probe (Fig. 7). The ECH conversion was abruptly accelerated and maximized to 98.25% ($x = 1.0$), and thereafter showed a slight decrease with the increasing 2MeIm/Co-BTC mass ratio, which was

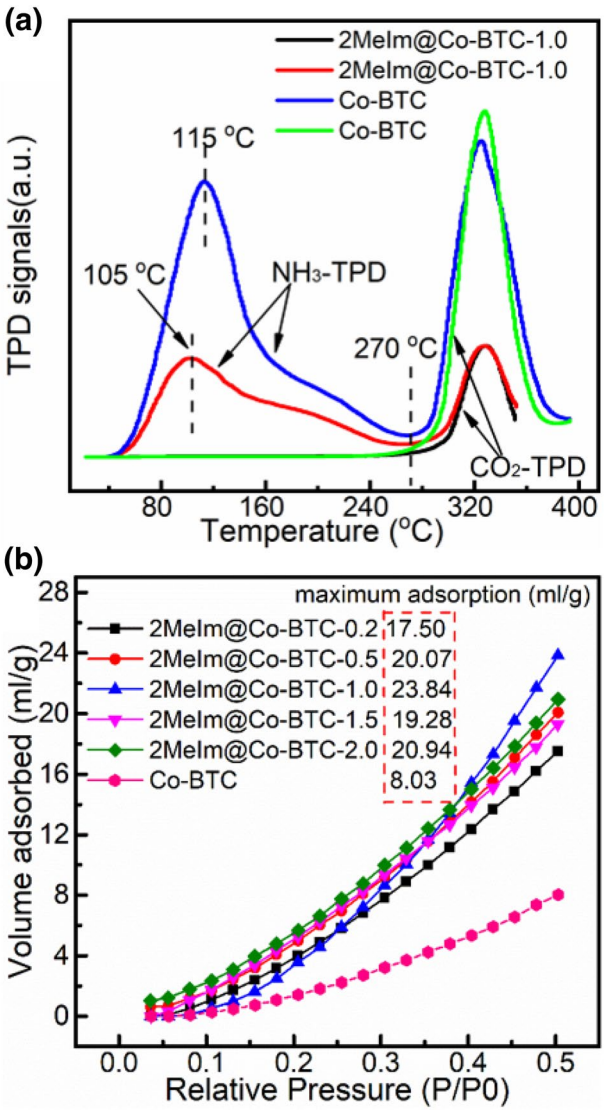

Fig. 6 CO_2/NH_3-TPD and CO_2-adsorption profiles of the 2MeIm@Co-BTC samples

due to the fact that the 2MeIm ligands within the modified Co-BTC played a great remarkable role in the surface area and pore structure increase. These make more Lewis acid sites exposure to the reactants, as a result, the catalytic activity was enhanced. In addition, such changes might be associated with the following reason: the sample prepared at low mass ratio ($x < 1.0$) cannot offer enough Lewis basic sites for CO_2 activation at the fixed time. For Co-BTC modified by excessive 2MeIm ($x > 1.0$, Fig. 6b), the excessive Lewis base within the structure could saturate the metal binding site, thus inhibiting the metal center's function for activating and opening of the ECH [47]. Besides, the selectivity to CPC presented an upward trend from 84.76% ($x = 0.2$) to 98.72% ($x = 2.0$), which was due to the decreasing amount of the coordinated water with increasing 2MeIm. As a result,

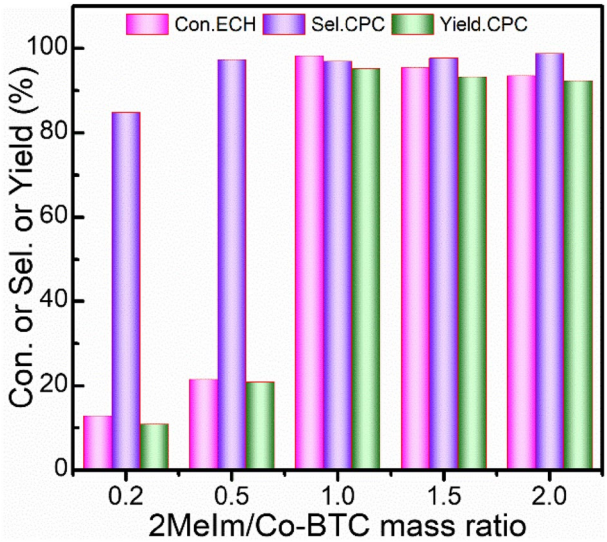

Fig. 7 The catalytic activity of the 2MeIm modified Co-BTC: ECH 20.0 g, reaction temperature (RETE) 100 °C, initial CO2 pressure (INCP) 3.0MPa, reaction time (RETI) 5 h, 0.5 wt% catalyst of ECH

the directional selectivity to CPC was enhanced followed with the decrease in ECH hydrolysis. The highest CPC yield of 95.21% was achieved over the sample with mass ratio of 1.0. Therefore, the 2MeIm@Co-BTC-1.0 was employed for the subsequent research.

Reaction temperature as a significant factor for determining the reaction process was usually investigated in the fixed catalytic system (Fig. 8a). It can be observed the conversion of ECH sharply increased from 59.65% (80 °C) to 94.43% (90 °C), followed by a slow rise to 98.25% (100 °C) and 99.54% (110 °C), while the CPC selectivity exhibited a downward trend with the increasing temperature. This was mainly due to the increasing release of residual water molecule with increasing reaction temperature, thereby resulting in the enhancement of ECH hydrolysis. Therefore, considering both factors (the energy consumption and product purity), 90 °C can be regarded as the optimal temperature for CO_2 conversion.

For the gas–liquid reaction, it was well-known that the reaction process can be efficiently promoted under the high-pressure system. Figure 8b showed the correlation between the carbon dioxide pressure and ECH yield. It undoubtedly known that the ECH consists of both forms (liquid and gas) at the setting temperature and high concentration of carbon dioxide supports the ECH conversion [48]. Nevertheless, ECH conversion was steeply-promoted from 45.55% (2.0 MPa) to the peak (95.43%, 3.0 MPa), suggesting that a higher concentration of carbon dioxide can effectively

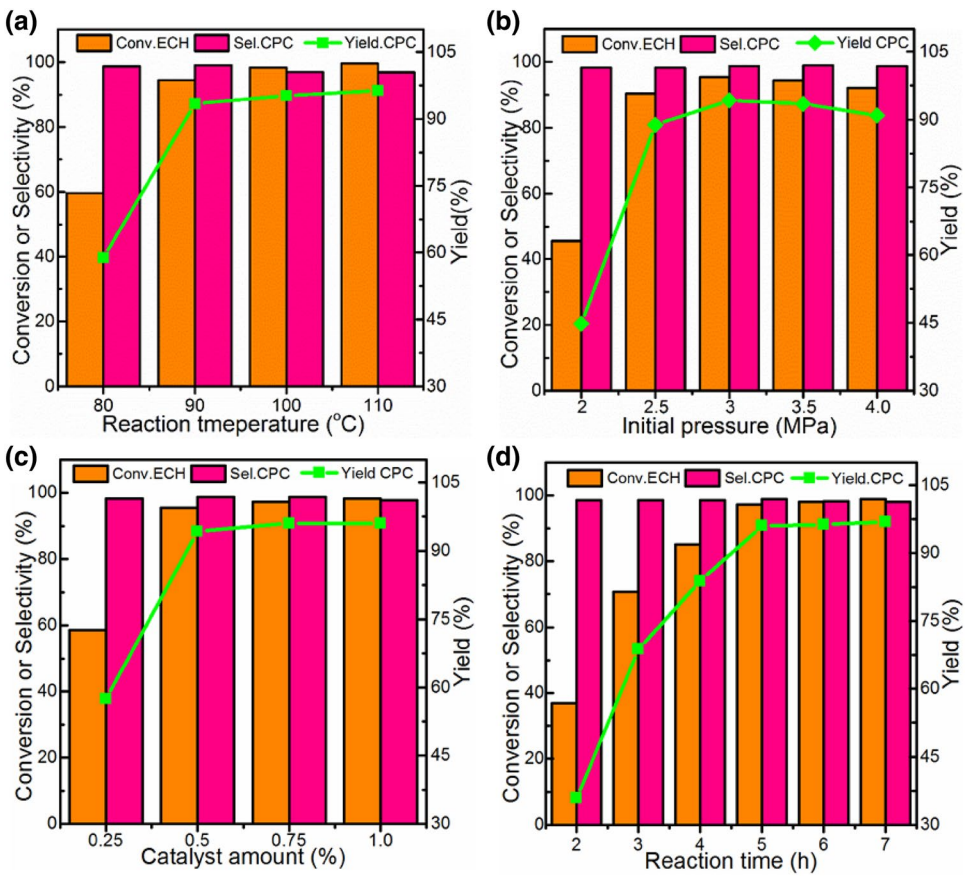

Fig. 8 **a** Effects of reaction temperature: ECH 20.0 g, INCP 3.0 MPa, RETI 5 h, 0.5 wt% catalyst of ECH. **b** Effects of initial pressure: ECH 20.0 g, RETE 90 °C, RETI 5 h, 0.5 wt% catalyst of ECH. **c** Effects of catalyst amount: ECH 20.0 g, INCP 3.0 MPa, RETE 90 °C, RETI 5 h. **d** Effects of reaction time: ECH 20.0 g, RETE 90 °C, INCP 3.0 MPa, 0.75 wt% catalyst of ECH. Initial CO_2 pressure (INCP), reaction time (RETI), reaction temperature (RETE)

enhance the solubility of CO_2 in ECH, while active molecules also increase during the CPC synthesis. However, the ECH conversion slightly decreased with the pressure above 3.0 MPa, indicating that a higher pressure may inhibit the interaction between reactants and catalyst (dilution effect) [49]. As a result, the low yield of CPC was gained. Thus, initial pressure of 3.0 MPa was more efficient for achieving a satisfactory conversion of ECH.

Appropriate concentration of active sites employed in the catalytic system can efficiently accelerate the conversion of carbon dioxide into cyclic carbonates. Figure 8c displayed the effects of the modified Co-BTC amount on the CPC yield. When the catalyst amount increased from 0.25 to 1.0 wt% of ECH, the conversion of ECH was steeply enhanced and then maintained a constant. This was likely related to the rapid increase of CPC and decrease in the amount of ECH during the catalytic process [50]. Besides, when there was an increase in the amount of catalyst, the selectivity to CPC displayed a slight drop, suggesting that the hydrolyzate (3-chloro-1,2-propanediol) increased during the catalytic process (Fig. S2, GC–MS). As a consequence, to obtain the high conversion of ECH with less catalyst amount, 0.75 wt% catalyst of ECH was considered as the most appropriate catalyst concentration for carbon dioxide conversion.

The correlation between reaction time and CPC yield was investigated via prolongation of reaction time (Fig. 8d). The conversion of ECH exhibited an abruptly upward trend from 36.87% (2 h) to 97.21% (5 h) and then displayed a slight increase (98.84%, 7 h), while the CPC selectivity presented a slight dip from 98.52% (2 h) to 98.05% (7 h), which was related to the hydrolysis of ECH with increasing time, and also in a good agreement with the results (Fig. 8a, c). Therefore, 5 h was the optimal reaction time for carbon dioxide conversion. According to the above analysis, the highest catalytic activity was achieved with 97.21% of ECH conversion and 98.79% of CPC selectivity under the optimal reaction conditions (3.0 MPa, 90 °C, 5 h, 0.75 wt% catalyst of ECH). Additionally, the kinetic law of the CO_2 chemical fixation was also studied in Fig. S3, with the first order kinetic being revealed for this coupling process.

2.3 Recyclability of the Catalyst

The recyclability as the important parameter for evaluating the catalytic performance is usually investigated through reusing the sample under the identical catalytic system (Fig. 9). The conversion of ECH decreased slightly from 98.25 to 90.59% after the modified Co-BTC was reused three times. Interestingly, the selectivity to CPC exhibited an upward trend from 96.91 to 98.10% when the sample was recovered after fourth times, a case that could be related to the gradual release of water molecule during the recovery

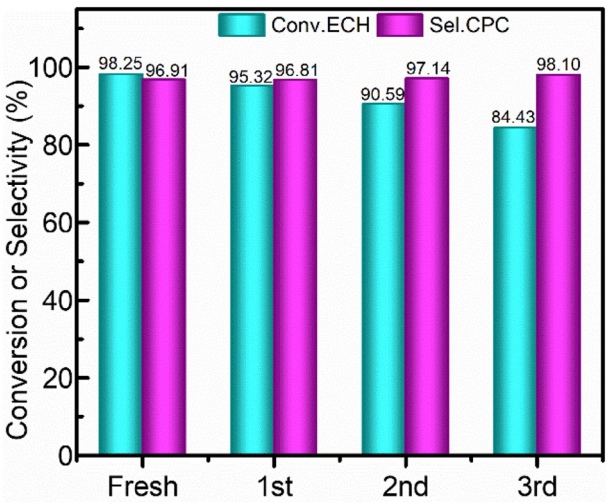

Fig. 9 The recyclability of the 2MeIm@Co-BTC-1.0 sample. Reaction conditions: ECH 20.0 g, RETE 100 °C, INCP 3.0 MPa, RETI 5 h, 0.75 wt% catalyst of ECH

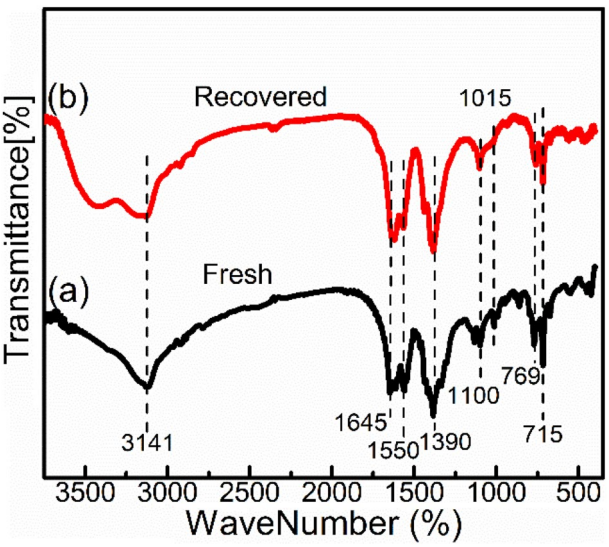

Fig. 10 FT-IR spectra of the recovered sample after three cycles

reactions (the residual amount of water molecule decreased together with the decrease in ECH hydrolysis). As a consequence, the selectivity to ECH increased when the catalyst was recovered several times. Besides, no obvious difference for both the fresh and recovered samples was observed in FT-IR spectra (Fig. 10), and only 1.90% lost rate for the employed catalyst was detected by ICP-OES (Table S2), indicating the sample was stable during the liquid reaction. Besides, the leaching tests were also performed as shown in Fig. S4, only a slight increase in ECH conversion was observed after the catalyst-free liquid was reperformed the coupling reaction, suggesting that the 2MeIm groups were

anchored within the Co-BTC via the newly-formed structure (Fig. 2). Besides, only a slight change in the crystal structure was detected for the recovered sample (Fig. S5), indicating that 2MeIm modified Co-BTC was stable during the coupling process.

2.4 Carbon Dioxide Coupling with Epoxide

To explore the applied scope of the modified Co-BTC for CO_2 conversion, some substrates such as ECH, allyl-glycidyl ether (AGE), 1, 2-epoxybutane (1, 2 EB) and propylene oxide (PO) were adopted as the probe molecules (Table 2). It can be observed that the 2MeIm modified Co-BTC can efficiently enhance the transformation of various epoxides into corresponding carbonates (^{1}H-NMR, Fig. S6). When PO was adopted as the substrate, the lowest conversion was obtained, which was mainly due to the low reactivity of propylene oxide molecule. However, when 1.0 wt% methanol of PO was added in the catalytic system, an obvious enhancement in conversion of PO was observed, which could be possibly due to the hydroxyl group of methanol promoting the ring opening of epoxide [51]. Besides, when CO_2 was chemically fixed with AGE as substrate, the selectivity to the corresponding carbonate was lowest, possibly due to the big steric hindrance of AGE among the studied epoxides [52], thereby making it difficult for the contact between carbon dioxide and AGE.

The existence of Lewis acid sites within the modified Co-BTC has been confirmed by NH_3-TPD profile (Fig. 6a). Besides, dimethylamine and 2MeIm cations within the crystal structure could serve as the Lewis base sites. Therefore, according to above analysis as well as the reported literatures [53, 54], a mechanism for catalytic conversion of CO_2 into cyclic carbonates over one possible framework structure was proposed (Scheme 2). The epoxide was firstly linked to the unsaturated Co atom (Lewis acid site), followed by the

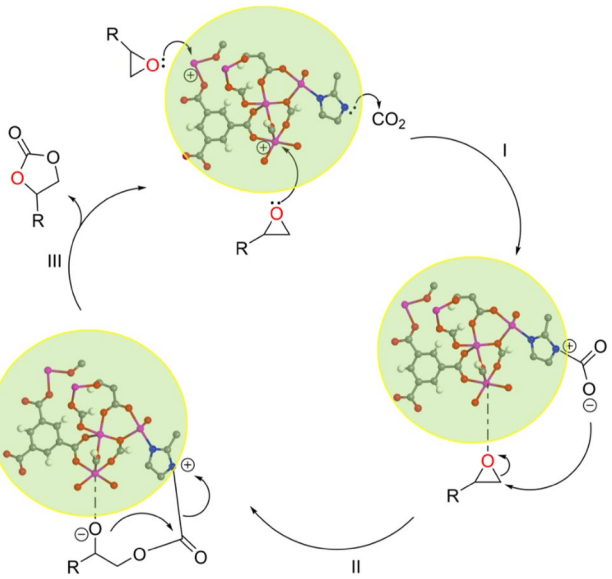

Scheme 2 A proposed mechanism for CO_2 coupling with epoxide over one possible framework structure of 2MeIm@Co-BTC

Table 2 Carbon dioxide cycloaddition with different epoxides

Entry	Epoxides	Cyclic carbonates	Con. (%)	Sel. (%)	Yie. (%)	Tem. (°C)
1	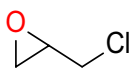	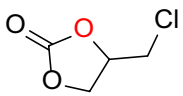	97.21	98.79	96.03	90
2		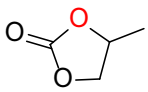	63.08	99.60	62.83	100
3[a]		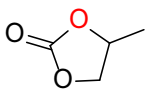	96.48	98.84	95.36	100
4	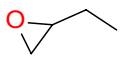	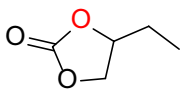	98.64	96.06	94.75	110
5	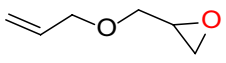	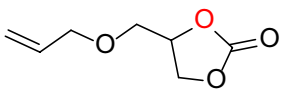	97.43	92.35	89.98	100

Epoxides 20.0 g, INCP 3.0 MPa, RETI 5 h, 0.75 wt% catalyst of the epoxides

[a]The reaction system was added with methanol (0.2 g)

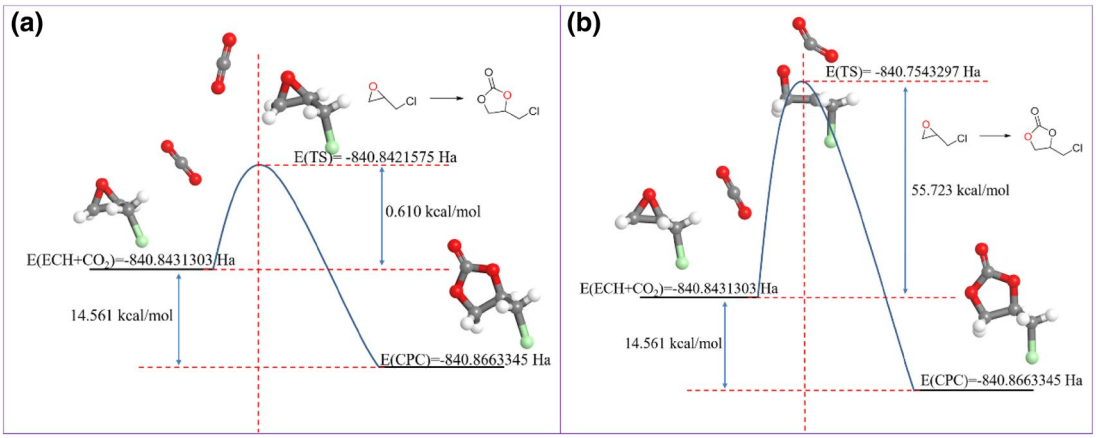

Fig. 11 The simulation results of transition state (TS) search for CO_2 coupling with ECH, the density function theory (DFT) calculations were performed with the use of the DMol3 Package (GGA, PBE) for structural optimization (ECH, CO_2, CPC) and transition state search

O atom of the activated carbon dioxide attacking the less sterically hindered carbon of the activating epoxide to form an intermediate (Fig. 11). Subsequently, the intermediate underwent a ring-close reaction. As a result, the modified Co-BTC was regenerated followed with the cyclic carbonate synthesis.

3 Conclusions

In this work, the modified Co-BTC was prepared via grafting 2-methylimidazole onto the surface of Co-BTC, which was further employed for catalytic conversion of CO_2 into cyclic carbonates. When 0.75 wt% catalyst of ECH was used in the catalytic system, 97.21% of ECH conversion and 98.79% of CPC selectivity were obtained over 2MeIm@Co-BTC-1.0 (3.0 MPa, 90 °C, 5 h). In addition, a new structure of hexagonal prisms appeared after Co-BTC was modified by 2-methylimidazole. N_2-adsorption analysis revealed the presence of micro- and meso-pores inside the modified Co-BTC. Additionally, this composite can efficiently convert various epoxides into cyclic carbonates. This work provides a method for designing a special material that can be used for efficient synthesis of cyclic carbonates with greenhouse gas as the starting raw.

Acknowledgments The work was financially supported by the National Natural Science Foundation of china (Nos. 21676054, 21406034), and Scientific Research Foundation of Graduate School of Southeast University (No. 3207049714).

References

1. Sarfraz M, Ba-Shammakh M (2016) J Taiwan Inst Chem Eng 65:427–436
2. Dai WL, Chen L, Yin SF, Li WH, Zhang YY, Luo SL, Au CT (2010) Catal Lett 137:74–80
3. Wang TF, Zheng DN, Ma Y, Guo JY, He ZP, Ma B, Liu LH, Ren TG, Wang L, Zhang JL (2017) J CO2 Util 22:44–52
4. Yang N, Wang R (2015) J Clean Prod 103:784–792
5. Zamani AH, Shohaimi NAM, Rosid SJM, Abdullah NH, Shukri NM (2019) J Taiwan Inst Chem Eng 96:400–408
6. Song QW, Zhou ZH, He LN (2017) Green Chem 19:3707–3728
7. Fan GZ, Luo SS, Fang T, Wu Q, Song GS, Li JF (2015) J Mol Catal A 404–405:92–97
8. Fan GZ, Zhao HT, Duan ZX, Fang T, Wan MH, He LN (2011) Catal Sci Technol 1:1138–1141
9. Xu H, Liu XF, Cao CS, Zhao B, Cheng P, He LN (2016) Adv Sci 3:1600048
10. Tamura M, Honda M, Noro K, Nakagawa Y, Tomishige K (2013) J Catal 305:191–203
11. Kumar P, Srivastava VC, Gläser R, With P, Mishra IM (2017) Powder Technol 309:13–21
12. Peng J, Yang HJ, Song NN, Guo CY (2015) J CO2 Util 9:16–22
13. Wu YF, Song XH, Zhang JH, Xu SQ, Gao LJ, Zhang J, Xiao GM (2019) Chem Eng Sci 201:288–297
14. Ghosh A, Ramidi P, Pulla S, Sullivan SZ, Collom SL, Gartia Y, Munshi P, Biris AS, Noll BC, Berry BC (2010) Catal Lett 137:1–7
15. Wang TF, Zheng DN, Zhang JS, Fan BW, Ma Y, Ren TG, Wang L, Zhang JH (2017) ACS Sustain Chem Eng 6:2574–2582
16. Goodrich P, Gunaratne HQN, Jacquemin J, Jin LL, Lei YT, Seddon KR (2017) ACS Sustain Chem Eng 5:5635–5641
17. Yue CT, Su D, Zhang X, Wu W, Xiao LF (2014) Catal Lett 144:1313–1321
18. Zheng DN, Zhang JS, Zhu XR, Ren TG, Wang L, Zhang JL (2018) J CO2 Util 27:99–106
19. Wu ZL, Xie HB, Yu X, Liu EH (2013) ChemCatChem 5:1328–1333
20. Tharun J, Mathai G, Kathalikkattil AC, Roshan R, Kwak JY, Park DW (2013) Green Chem 15:1673
21. Xue ZM, Zhao XH, Wang JF, Mu TC (2017) Chemistry 12:2271–2277
22. Xie Y, Wang TT, Yang RX, Huang NY, Zou K, Deng WQ (2014) Chemsuschem 7:2110–2114
23. Monassier A, D'Elia V, Cokoja M, Dong HL, Pelletier JDA, Basset JM, Kühn FE (2013) ChemCatChem 5:1321–1324
24. Tiffner M, Gonglach S, Haas M, Schçfberger W, Waser M (2017) Chemistry 12:1048–1051

25. Chang HB, Li QS, Cui XM, Wang HX, Bu ZW, Qiao CZ, Lin T (2018) J CO2 Util 24:174–179
26. Buonerba A, De Nisi A, Grassi A, Milione S, Capacchione C, Vagin S, Rieger B (2015) Catal Sci Technol 5:118–123
27. Zhi YF, Mu JL, Shan SY, Su HY, Wu SS, Jia QM (2016) J Taiwan Inst Chem Eng 61:351–355
28. Tambe PR, Yadav GD (2017) Clean Technol Environ Policy 20:345–356
29. Jeong HM, Roshan R, Babu R, Kim HJ, Park DW (2017) Korean J Chem Eng 35:438–444
30. Song JL, Zhang ZF, Hu SQ, Wu TB, Jiang T, Han BX (2009) Green Chem 11:1031–1036
31. Mousavi B, Chaemchuen S, Moosavi B, Luo ZX, Gholampour N, Verpoort F (2016) New J Chem 40:5170–5176
32. Miralda CM, Macias EE, Zhu MQ, Ratnasamy P, Carreon MA (2012) ACS Catal 2:180–183
33. Jang MS, Lee YR, Ahn WS (2015) Bull Korean Chem Soc 36:363–366
34. Kim SN, Kim J, Kim HY, Cho HY, Ahn WS (2013) Catal Today 204:85–93
35. Zanon A, Chaemchuen S, Mousavi B, Verpoort F (2017) J CO2 Util 20:282–291
36. Wu YF, Song XH, Li S, Zhang JH, Yang XH, Shen PX, Gao LJ, Wei RP, Zhang J, Xiao GM (2018) J Ind Eng Chem 58:296–303
37. Kwon HT, Jeong HK, Lee AS, An HS, Lee JS (2015) J Am Chem Soc 137:12304–12311
38. Groen JC, Peffer LAA, Moulijn JA, Pérez-Ramírez J (2004) Colloids Surf A 241:53–58
39. Sun ZH, Yu WT, Cheng XF, Wang XQ, Zhang GH, Yu G, Fan HL, Xu D (2008) Opt Mater 30:1001–1006
40. Zeng GJ, Chen Y, Chen L, Xiong PX, Wei MD (2016) Electrochim Acta 222:773–780
41. Sun KK, Li L, Yu XL, Liu L, Meng QT, Wang F, Zhang R (2017) J Colloid Interface Sci 486:128–135
42. Sánchez-Andújar M, Gómez-Aguirre LC, Pato Doldán B, Yáñez-Vilar S, Artiaga R, Llamas-Saiz AL, Manna RS, Schnelle F, Lang M, Ritter F, Haghighirad AA, Señarís-Rodríguez MA (2014) CrystEngComm 16:3558
43. Singh MP, Dhumal NR, Kim HJ, Kiefer J, Anderson JA (2016) J Phys Chem C 120:17323–17333
44. Wang PC, Zhou YK, Hu M, Chen J (2017) Appl Surf Sci 392:562–571
45. Gowthaman NSK, Sinduja B, Karthikeyan R, Rubini K, Abraham John S (2017) Biosens Bioelectron 94:30–38
46. Fu Y, Su J, Yang SH, Li GB, Liao FH, Xiong M, Lin JH (2010) Inorg Chim Acta 363:645–652
47. Paddock RL, Hiyama Y, McKay JM, Nguyen ST (2004) Tetrahedron Lett 45:2023–2026
48. Wu SS, Zhang XW, Dai WL, Yin SF, Li WS, Ren YQ, Au CT (2008) Appl Catal A 341:106–111
49. Han LN, Choi HJ, Kim DK, Park SW, Liu BY, Park DW (2011) J Mol Catal A 338:58–64
50. Bai DS, Jing HW, Wang GJ (2012) Appl Organomet Chem 26:600–603
51. Song XH, Wu YF, Pan DH, Wei RP, Gao LJ, Zhang J, Xiao GM (2018) J CO2 Util 24:287–297
52. Miao CX, Wang JQ, Wu Y, Du Y, He LN (2008) Chemsuschem 1:236–241
53. Song LL, Zhang XL, Chen C, Liu XL, Zhang N (2017) Microporous Mesoporous Mater 241:36–42
54. He HM, Perman JA, Zhu GS, Ma SQ (2016) Small 12:6309–6324

Affiliations

Yuanfeng Wu[1] · Xianghai Song[1] · Siquan Xu[1] · Jiahui Zhang[1] · Yanli Zhu[1] · Lijing Gao[1] · Guomin Xiao[1]

✉ Guomin Xiao
xiaogm426@gmail.com

[1] School of Chemistry and Chemical Engineering, Southeast University, Nanjing 211189, China